# A Risk-Based Modeling Approach for Radiation Therapy Treatment Planning Under Tumor Shrinkage Uncertainty

Gino J. Lim[a,*], Laleh Kardar[b], Saba Ebrahimi[a], Wenhua Cao[c]

[a]*Department of Industrial Engineering, University of Houston, 4800 Calhoun Road, Houston, TX 77204, USA.*
[b]*PROS Revenue Management, Houston, TX 77002, USA.*
[c]*Department of Radiation Physics, The University of Texas MD Anderson Cancer Center, Houston, TX 77030, USA*

**Abstract**

Robust optimization approaches have been widely used to address uncertainties in radiation therapy treatment planning problems. Because of the unknown probability distribution of uncertainties, robust bounds may not be correctly chosen, and a risk of undesirable effects from worst-case realizations may exist. In this study, we developed a risk-based robust approach, embedded within the conditional value-at-risk representation of the dose-volume constraint, to deal with tumor shrinkage uncertainty during radiation therapy. The objective of our proposed model is to reduce dose variability in the worst-case scenarios as well as the total delivered dose to healthy tissues and target dose deviations from the prescribed dose, especially, in underdosed scenarios. We also took advantage of adaptive radiation therapy in our treatment planning approach. This fractionation technique considers the response of the tumor to treatment up to a particular point in time and re-optimizes the treatment plan using an estimate of tumor shrinkage. The benefits of our model were tested in a clinical lung cancer case. Four plans were generated and compared: static, nominal-adaptive, robust-adaptive, and conventional robust (worst-case) optimization. Our results showed that the robust-adaptive model, which is a risk-based model, achieved less dose variability and more control on the worst-case scenarios while delivering the prescribed dose to the tumor target and sparing organs at risk. This model also outperformed other models in terms of tumor dose homogeneity and plan robustness.

*Keywords:* OR in Medicine, Radiation Therapy Planning, Tumor Shrinkage, Risk Management, CVaR

## 1. Introduction

### *1.1. Background*

Lung cancer remains the leading cause of cancer-related death in the United States (Siegel et al., 2018). For patients wtih non-small cell lung cancer (NSCLC), the most common type of lung cancer, radiation therapy (RT) is a common treatment modality. High doses of radiation are required to eradicate lung tumors, so the surrounding normal tissue requires maximal protection

*Corresponding author
*Email addresses:* ginolim@uh.edu (Gino J. Lim ), lale.kardar@gmail.com (Laleh Kardar), sebrahimi@uh.edu (Saba Ebrahimi), WCao1@mdanderson.org (Wenhua Cao)

(Li et al., 2014; Kardar et al., 2014). In intensity-modulated radiation therapy (Lim and Cao, 2012; Lin et al., 2016), one of the most commonly used types of RT for lung cancer, each beam of radiation is partitioned into a large set of "beamlets" that have individually adjustable intensities. The intensity maps for each beam are calculated using an "inverse" treatment planning system that uses optimization approaches wherein the beam intensities are defined as decision variables. The objective function of the inverse plan determines how best to deliver the desired dose to the target while minimizing the dose to normal tissues.

In RT, various uncertain factors can negatively affect the outcomes of treatment, such as internal organ motion (Olafsson and Wright, 2006), nonrigid deformation of organs (Bortfeld et al., 2002), set-up and positioning errors (Stroom and Heijmen, 2002; Sir et al., 2012), and tumor shrinkage (Erridge et al., 2003). A common technique used to handle these uncertainties in RT treatment planning is robust optimization (RO) (Chu et al., 2005; Bortfeld et al., 2008; Chan et al., 2006; Chen et al., 2012). The vast majority of clinically oriented RO approaches are based on the *min-max*, which focuses on minimizing the worst-case scenario (Gabrel et al., 2014; Aven, 2016). However, many of these methods do not explicitly consider changes in tumor geometry during treatment.

Several studies have reported a wide range of decreases in tumor volume using computed tomography (CT) data sets (Woodford et al., 2007; Knap et al., 2010). Kupelian et al. (2005) reported a mean tumor shrinkage rate and showed that the rate of volume change was relatively constant throughout the course of treatment. In studies of patients with NSCLC, the gross tumor volume (GTV) decreased by various proportions (Britton et al., 2007; Fox et al., 2009). These varying degrees of tumor shrinkage raise the question of how best to adapt RT treatment plans.

Adaptive radiation therapy (ART) is a treatment planning method that makes systematic treatment adjustments in response to changes that occur between treatments and during the course of treatments. The literature shows that using ART improves treatment quality in terms of normal-tissue sparing and tumor-cell reduction (Schoot et al., 2017; Ramella et al., 2017). Other studies have demonstrated the benefits of ART in terms of cost and time (Dial et al., 2016; Veresezan et al., 2017). Veresezan et al. (2017) recommended that ART error calculations and imaging studies should be repeated to verify treatment accuracy, but this can be a time-consuming process. Because imaging the patient at every visit during the treatment period can be costly, in practice, trade-offs must be made among costs, timing, and the recommended number of adaptive plans. Therefore, finding the optimal timing for adaptation is necessary to improve the clinical feasibility of ART.

Several approaches have been proposed to optimally determine how often to conduct adaptation during treatment, focusing on target-volume reduction (Saka et al., 2011; Guckenberger et al., 2011a; Belfatto et al., 2016) and the amount of dose per volume received at the tumor (Zheng et al., 2015; Lee et al., 2014; Berkovic et al., 2015; Zarepisheh et al., 2014). For example, Saka et al. (2011) developed an image-based adaptive intensity-modulated radiation therapy (IMRT) optimization approach in which they proposed adaptation once before fraction 25 and once after fraction 25 on the basis of the latest tumor geometry information. Guckenberger et al. (2011a) proposed adapting the plan once or twice in week 3 or 5 for NSCLC treatment. Zheng et al. (2015) proposed that the plan adaptation for lung cancer treatment should occur at the $15^{th}$ fraction. They also showed that the adaptation point should be before the $31^{st}$ fraction to provide the most clinical benefit. Berkovic et al. (2015) demonstrated that adaptation performed around fraction 15 was most beneficial in IMRT for lung cancer.

Some studies have explored the advantages of combining adaptation with robust optimization in RT treatment planning. Chan and Mišić (2013) developed a framework that integrated ART and RO techniques for lung cancer IMRT treatment planning under breathing motion uncertainty. They also presented an approach to adapt the uncertainty set after each fraction based on the patient's daily breathing pattern. Later, Mišić and Chan (2015) showed that their previous approach (Chan and Mišić, 2013) led to a desirable homogeneity in tumor dose. However, they did not consider changes in tumor geometry during the treatment.

### *1.2. Risk-based Modeling*

RO is a common technique for handling uncertainties in RT treatment planning such as tumor shrinkage uncertainty. In RO, an uncertainty set must be defined for the unknown parameter in the optimization model. However, because the probability distribution of the tumor shrinkage is unknown, robust bounds may not be accurately defined. As a result, many instances in the worst case can lead to undesirable effects in the optimal solution. Figure 1 illustrates the robust bounds (i.e., dose lower/upper bounds) and the expected worst cases (i.e., underdosed/overdosed worst cases) in RT planning problems. Here, we specifically focus on underdosed worst cases, which are highly undesirable due to the risk of tumor recurrence if areas of malignant cells are left undertreated or untreated.

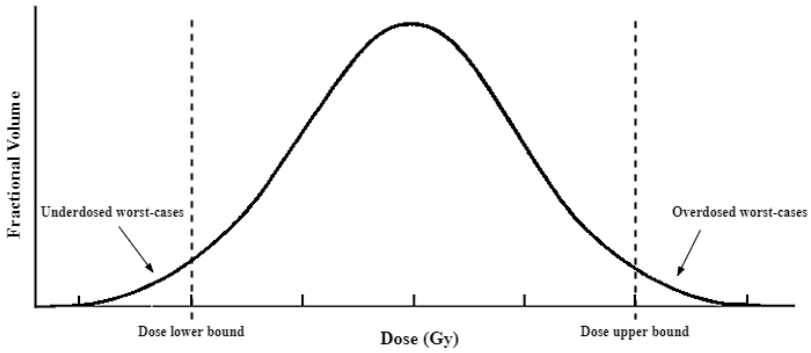


Figure 1: Representation of the expected tail loss in delineation of worst cases

Recent studies have discussed the importance of risk management in decision-making in the presence of uncertainty (Ben-Haim, 2012; Li et al., 2018). Several risk-based modeling approaches have addressed the problem of reducing variability, including the value-at-risk (VaR), conditional value-at-risk (CVaR), and chance constraint approaches (Zaghian et al., 2017b; Khabazian et al., 2019). To deal with the risk of having worst-case outcomes resulting from uncertainties in RT treatment planning, we used a CVaR approach. CVaR is one of the most commonly used risk models; it has been applied to several problems dealing with high risks, such as operating room scheduling (Najjarbashi and Lim, 2019), power flow optimization (Summers et al., 2015), energy storage (Moazeni et al., 2015), disaster management (Noyan, 2012), and water allocation (Hu et al., 2016), to mitigate risk and achieve risk-averse solutions. Most studies have reported that efficient worst-case risk management can be achieved with the CVaR approach (Uryasev, 2000; Summers et al., 2015). Furthermore, because of the tractability of CVaR-based models, it has also been used to develop RT treatment planning optimization models (Romeijn et al., 2003, 2006; Chan et al.,

2014; An et al., 2017). Using CVaR, one can optimize the expected tail loss – the underdosed or overdosed voxels (Figure 1) – while minimizing the negative effects on worst cases.

### *1.3. The Problem Scope*

This paper aims to use CVaR to investigate the potential advantages of using an adaptive fractionation scheme while considering tumor volume changes over time. The objective of our robust-adaptive model is to reduce dose variability in the worst-case scenarios, dose to healthy tissues, and discrepancies between the dose received by the target and the prescribed dose, especially, in underdosed scenarios. The proposed adaptive planning technique reoptimizes the treatment plan after delivering a subsequence of fractions by incorporating an estimate of the tumor shrinkage that might have occurred during the previous fractions. The exact tumor shrinkage rate is not known beforehand, and it can be variable and patient-dependent. Thus, one major challenge in our adaptive planning methodology is determining the actual tumor shrinkage rate with which to update the residual tumor volume over time. If the treatment is planned based on a specific shrinkage rate but the tumor shrinks at a lower rate, the tumor may end up being underdosed, and the quality of the treatment may be greatly compromised. Likewise, if the tumor regresses at a higher rate than the planned rate, then healthy tissue sparing will be poorly controlled.

To overcome this challenge, we approximate the residual tumor volume using multiple estimated tumor volumes, each of which corresponds to a possible rate of tumor shrinkage. Each estimated tumor volume is associated with a probability, and the uncertainty inherent in the probability is accounted for through an RO approach. The risk-based RO model, embedded within the CVaR representation of the dose-volume constraint, uses these tumor volume estimates to optimize a plan for all estimates simultaneously. The robust counterpart of the problem is a linear programming problem that is computationally tractable. The output of this model was compared to that of static (nonadaptive), nominal-adaptive, and RO models. The clinical advantage of this method is that it has the potential to reduce the dose burden on healthy tissue while satisfying therapeutic requirements for tumor coverage. Also, this risk-based model reduces variability and the negative impacts of worst cases.

The rest of this paper is organized as follows. In Section 2, we explain how CVaR constraints can be used to model dose-volume constraints in RT. We then develop an approach to nominal and robust-adaptive IMRT treatment planning in the presence of tumor shrinkage uncertainty and provide the associated mathematical formulations. Section 3 provides results from our experimental study using clinical lung cancer patient data. We conclude the paper in Section 4.

## 2. Risk-based RT Planning Using CVaR

### *2.1. Problem Description and Notation*

In RT plans, given a predetermined set of beams, the aperture of a beam is decomposed into small beamlets. Let $B$ denote the set of all beamlets. The primary decision variables of the optimization model are the beamlet weights $w_b$, representing the intensity of radiation delivered by beamlet $b$, where $b \in B$. In general, we will consider two types of treatment regions: the target(s) or planning target volume (PTV) and the organs at risk (OARs). We denote the set of target structures by $T$ and the set of OARs by $S$. In practice, each structure $s \in T \cup S$ is discretized into a finite number of cubes $V_s$, which are known as voxels. Often, some structures overlap in the image. For example, if a target has invaded an OAR, some voxels will be in both the target and the OAR. In

such a case, a dominant structure will be defined for those voxels on the basis of a priority list of all structures (i.e., targets usually have the highest priorities, followed by OARs). Let $D_v$ denote the total dose that a voxel $v$ receives. We make the standard assumption that $D_v$ can be expressed as a linear combination of the individual beamlet intensities. Thus, $D_v$ can be calculated as

$$D_v = \sum_{b \in B} \Delta_{v,b} \cdot w_b \qquad \forall v \in V_s, \quad s \in T \cup S, \tag{1}$$

where $\Delta_{v,b}$ is the element of the dose deposition matrix defined as the dose delivered to voxel $v$ by beamlet $b$ at unit intensity.

We next explain the development of the CVaR constraint (Chan et al., 2014). For convenience, we will first define the loss function to define the dose-volume constraint using the CVaR methodology. For all structures, the corresponding loss function is the dose calculation function itself because very high dose levels are undesirable. Let $H_s(\zeta; \mathbf{w})$ denote the fraction of $V_s$ that receives more than $\zeta$ dose given radiation intensities $\mathbf{w}$:

$$H_s(\zeta; \mathbf{w}) = \frac{|\{v \in V_s \,|D_v \geq \zeta\}|}{|V_s|}. \tag{2}$$

The upper VaR at level $\alpha$ (upper $\alpha$-VaR) is defined as the smallest dose level such that no more than $100(1-\alpha)\%$ of structure $s$ receives a higher dose. The upper $\alpha$-VaR for structure s, $\bar{\zeta}_s^{\alpha}$, is defined as

$$\bar{\zeta}_s^{\alpha} = \min\{\zeta \mid H_s(\zeta; \mathbf{w}) \leq 1 - \alpha\}, \tag{3}$$

The upper CVaR at level $\alpha$ (upper $\alpha$-CVaR) is then the average of all doses that exceed the $\alpha$-VaR. The upper $\alpha$-CVaR for structure $s$, $\bar{\phi}_s^{\alpha}(\mathbf{w})$, is defined as

$$\bar{\phi}_s^{\alpha}(\mathbf{w}) = \min_{\zeta \in R} \left\{ \zeta + \frac{1}{(1-\alpha)|V_s|} \sum_{v \in V_s} (D_v - \zeta)^+ \right\}, \tag{4}$$

or equivalently

$$\bar{\phi}_s^{\alpha}(\mathbf{w}) = \bar{\zeta}_s^{\alpha} + \frac{1}{(1-\alpha)|V_s|} \sum_{v \in V_s} \left(D_v - \bar{\zeta}_s^{\alpha}\right)^+. \tag{5}$$

Similarly, lower CVaR constraints can be defined for target structures as

$$\underline{\phi}_s^{\alpha}(\mathbf{w}) = \underline{\zeta}_s^{\alpha} - \frac{1}{(1-\alpha)|V_s|} \sum_{v \in V_s} \left(\underline{\zeta}_s^{\alpha} - D_v\right)^+. \tag{6}$$

In the following sections, we explain RT optimization models that utilize CVaR constraints to impose dose-volume constraints on structures.

### 2.2. Static Model

Throughout this paper, we refer to the model developed by Chan et al. (2014) as the "static model" because it optimizes the beamlet intensities under the assumption that organ structure volumes remain unchanged during the treatment period; hence, it does not adapt to changes in the tumor geometry. It is used for comparison purposes. Details of this model are given in Appendix A.

### 2.3. Adaptive RT Scheme

#### 2.3.1. Scenario Generation for Tumor Shrinkage

In this section, we introduce a model that incorporates the temporal evolution of the tumor in response to radiation. We assume that the individual patient's tumor volume during the treatment can be approximated with multiple estimates of tumor volumes, each of which corresponds to a possible rate of tumor shrinkage. Suppose that there are $K$ estimates used in the approximation. Each of these instances is associated with a probability $p_k$, $k = 1, 2, ..., K$, where $\sum_{k=1}^{K} p_k = 1$.

To get multiple estimates of tumor volume, one needs to know the probability of the tumor volume estimates. Our starting point is a nominal probability mass function (PMF), and it is constructed from historical data showing rates of tumor shrinkage during the course of treatment in a pool of over 70 patients collected from the literature (Britton et al., 2007; Kupelian et al., 2005; Fox et al., 2009; Woodford et al., 2007; Guckenberger et al., 2011b). All of these studies showed that an NSCLC tumor shrinks at an approximately constant rate following the standard treatment with a fixed radiation dose (e.g., 2 Gy per fraction) throughout the treatment. The PMF of the tumor shrinkage rate specifies the likelihood of each rate of tumor shrinkage (or equivalently, each tumor volume estimate) during the course of treatment.

Figure 2 shows the tumor shrinkage rates per day plotted against initial tumor volumes for the patient population. We selected $K$ representative shrinkage rates to simulate the tumor volume changes that are likely to occur during the course of treatment. The probability distribution was constructed by first dividing the observed range into $K$ intervals (bins) and then calculating the number of shrinkage rates occurring in each interval.

#### 2.3.2. ART Approach

In the adaptive treatment planning method that we propose, the treatment is split into several epochs, and each epoch consists of multiple fractions. Different plans are used for each epoch. The treatment plan is adapted to the geometrical changes of the tumor after delivery of each epoch. The first epoch starts at the beginning of the treatment, at which point no shrinkage has yet been observed; therefore, the optimization for this epoch uses the original tumor volume. In the rest of the epochs, tumor shrinkage is reflected by removing a subset of healed voxels in the tumor region. Then, the updated tumor volume is used for the reoptimization. Thus, in our approach, the treatment plans are adapted in the following way. During the first epoch, the target is irradiated with a beamlet intensity vector obtained by solving the static model on the basis of the original tumor volume data. After the first epoch is delivered, a new data set corresponding to different tumor volume estimates is generated. The nominal model is then solved with this a new data set, leading to a new beamlet intensity vector to be used for the next treatment epoch. This process is repeated for each epoch until the end of the treatment. This procedure is presented as Algorithm 1. A similar ART approach was presented by Chan and Mišić (2013) for lung cancer IMRT treatment planning

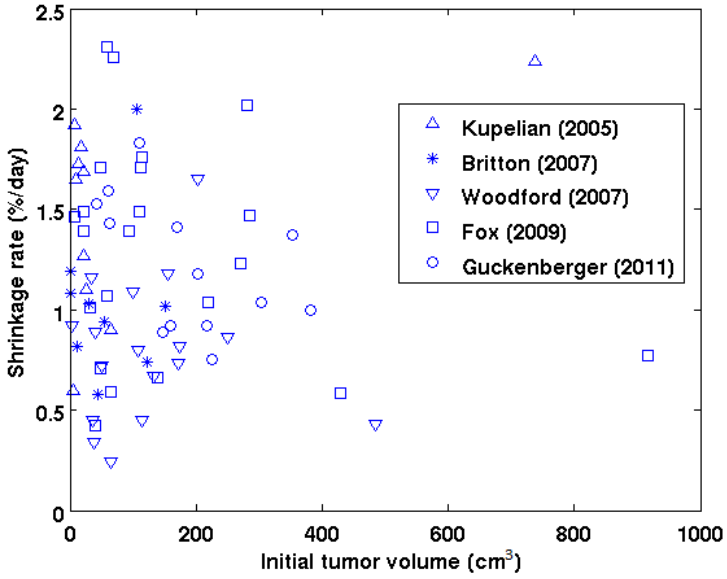


Figure 2: Scatterplot of tumor shrinkage rates at different initial tumor volumes

under breathing motion uncertainty, in which the uncertainty set is updated after each fraction using the daily breathing pattern. However, we consider multiple time epochs, and adaptation occurs after delivering multiple dose fractions because the reduction in tumor volume after one fraction is not noticeably different from the previous one in practice.

**Algorithm 1** Adaptive optimization method

**Input:** Total number of fractions ($N$), initial data set, number of treatment epochs ($m$), number of fractions in each treatment epoch$\{N_1, N_2, ..., N_m\}$;
Solve the static model using the original data to obtain a beamlet intensity vector $\mathbf{w}^0$
Deliver $\frac{\mathbf{w}^0}{N}$ to the patients for ($N_1$) fractions
Initialize j=2
**while** $j \leq m$ **do**
    Generate data set for different tumor shrinkage instances by modifying the tumor volume
    Solve the nominal model (B.1) with new data set (tumor volume) to obtain a new beamlet intensity vector $\mathbf{w}^j$
    Deliver $\frac{\mathbf{w}^j}{N}$ to the patient for ($N_j$) fractions
    $j \leftarrow j + 1$;
**end while**

*2.3.3. Nominal-Adaptive Treatment Planning*

In this section, we will explain how tumor volume changes can be incorporated into the optimization model using the nominal PMF of tumor shrinkage rates. The dose deposition matrix depends on the organ's position with respect to the beams. Considering tumor shrinkage allows us to shrink the beams, thereby reducing the dose to healthy tissue surrounding the target. Therefore, once the estimated tumor volumes are determined, a dose deposition matrix is calculated for each

estimate and the resulting matrices $\Delta_{v,k,b}$ are stored, where $\Delta_{v,k,b}$ is the dose delivered to voxel $v$ by beamlet $b$ at unit intensity for instance $k$.

Note that targets contain a different number of voxels in each estimate, and as a result, varying numbers of OAR voxels may overlap with targets. Therefore, the CVaR definition should be adjusted to reflect the varying number of voxels for each estimate. The upper $\alpha$-CVaR is then the sum of upper tail doses under each tumor shrinkage estimate weighted by the probability of the estimate's occurrence. The upper $\alpha$-CVaR is defined as

$$\bar{\phi}_s^{\alpha}(\mathbf{w}) = \bar{\zeta}_s^{\alpha} + \frac{1}{(1-\alpha)} \sum_{k \in K} \left( \frac{1}{|V_s^k|} \sum_{v \in V_s^k} \left( \sum_{b \in B} \Delta_{v,k,b} w_b - \bar{\zeta}_s^{\alpha} \right)^+ \right) p(k),$$

where $V_s^k$ denotes the number of voxels in structure $s$ for instance $k$.

Accounting for tumor shrinkage and using the nominal PMF of the instances, the nominal formulation is shown in Appendix B. Nominal-adaptive treatment planning is performed as in Algorithm 1, where the set of voxels $V_s^k$ is updated for reoptimization at each epoch.

### *2.4. Robust-Adaptive Treatment Planning*

If the realized tumor shrinkage deviates far from the estimates, the nominal-adaptive solution may result in an unacceptable dose distribution with hot and cold spots. For this reason, a robust formulation is needed to mitigate the uncertainty in the tumor shrinkage during the treatment. The goal is to find the beamlet intensity vector that minimizes the objective function while satisfying the constraints under any realization of the tumor shrinkage rate. The uncertainty set is determined before the treatment, and the robust optimization problem corresponding to this uncertainty set is solved. In this paper, we assume that the uncertainty in the tumor shrinkage rate can be reflected by changes in the nominal PMF of the representative shrinkage rates. We assume that the actual PMF, $\tilde{p}$, can deviate from the nominal PMF and is known to belong to an uncertainty set $P$ representing the set of possible PMFs, i.e., $\tilde{p} \in P$, and satisfies

$$p(k) - \underline{p}(k) \leq \tilde{p}(k) \leq p(k) + \bar{p}(k) \qquad \forall k \in K,$$

where $\underline{p}(\cdot)$ and $\bar{p}(\cdot)$ denote bounds on the difference between the nominal and the realized probability distribution (Bortfeld et al., 2008). Using the linear programming duality, upper-bound and lower-bound constraints are transformed into an equivalent linear formulation (Chan et al., 2014). Note that a different set of voxels $V_s^k$ is used for each tumor shrinkage scenario. The dose deviations from upper and lower $\alpha$-VaR for each voxel also vary for different tumor shrinkage scenarios (i.e., $\bar{d}_{v,k,\alpha}$ and $\underline{d}^s_{v,k,\alpha}$ ). As a result, the robust optimization model with CVaR constraints is

$$\min \quad \sum_{k \in K} \sum_{s \in \{T \cup S\}} \frac{C_s}{|V_s^k|} \sum_{v \in V_s^k} \sum_{b \in B} \Delta_{v,k,b} p(k) w_b \tag{7}$$

s.t.

$$\bar{\zeta}_s^{\alpha} + \frac{1}{1-\alpha} \left( \sum_{k \in K} \sum_{v \in V_s^k} \bar{d}^s_{v,k,\alpha} \frac{p(k)}{|V_s^k|} - \sum_{k \in K} \sum_{v \in V_s^k} \bar{d}^s_{v,k,\alpha} \frac{\underline{p}(k)}{|V_s^k|} + \sum_{k \in K} r_k^{\alpha,s} + \sum_{k \in K} \underline{p}(k) q^{\alpha,s} \right) \leq U_{\alpha}^s,$$

$$\forall \alpha \in \bar{A}_s, s \in \{T \cup S\},$$

$$\bar{d}^s_{v,k,\alpha} \geq \sum_{b \in B} \Delta_{v,k,b} w_b - \bar{\zeta}^\alpha_s, \quad \forall v \in V^k_s, \alpha \in \bar{A}_s, s \in \{T \cup S\}, k \in K,$$

$$q^{\alpha,s}(\bar{p}(k) + \underline{p}(k)) + r^{\alpha,s}_k - \sum_{v \in V^k_s} \frac{\bar{d}^s_{v,k,\alpha}}{|V^k_s|}(\bar{p}(k) + \underline{p}(k)) \geq 0, \quad \forall \alpha \in \bar{A}_s, s \in \{T \cup S\}, k \in K,$$

$$\underline{\zeta}^\alpha_s - \frac{1}{1-\alpha}\left(\sum_{k \in K}\sum_{v \in V^k_s} \underline{d}^s_{v,k,\alpha}\frac{p(k)}{|V^k_s|} - \sum_{k \in K}\sum_{v \in V^k_s} \underline{d}^s_{v,k,\alpha}\frac{\underline{p}(k)}{|V^k_s|} + \sum_{k \in K} r^{\alpha,s}_k + \sum_{k \in K} \underline{p}(k) q^{\alpha,s}\right) \geq L^s_\alpha,$$

$$\forall \alpha \in \underline{A}_s, s \in \{T \cup D\},$$

$$\underline{d}^s_{v,k,\alpha} \geq \underline{\zeta}^\alpha_s - \sum_{b \in B} \Delta_{v,k,b} w_b, \quad \forall v \in V^k_s, \alpha \in \underline{A}_s, s \in \{T \cup D\}, k \in K,$$

$$q^{\alpha,s}(\bar{p}(k) + \underline{p}(k)) + r^{\alpha,s}_k - \sum_{v \in V^k_s} \frac{\underline{d}^s_{v,k,\alpha}}{|V^k_s|}(\bar{p}(k) + \underline{p}(k)) \geq 0, \quad \forall \alpha \in \underline{A}_s, s \in \{T \cup D\}, k \in K,$$

$$\bar{\zeta}^\alpha_s \geq 0, \quad \forall \alpha \in \bar{A}_s, s \in \{T \cup S\},$$

$$\bar{d}^s_{v,k,\alpha} \geq 0, \quad \forall v \in V^k_s, \alpha \in \bar{A}_s, s \in \{T \cup S\}, k \in K,$$

$$\underline{\zeta}^\alpha_s \geq 0, \quad \forall \alpha \in \underline{A}_s, s \in \{T \cup D\},$$

$$\underline{d}^s_{v,k,\alpha} \geq 0, \quad \forall v \in V^k_s, \alpha \in \underline{A}_s, s \in \{T \cup D\} k \in K,$$

$$r^{\alpha,s}_k \geq 0, \quad \forall \alpha \in \bar{A}_s \cup \underline{A}_s, s \in \{T \cup S \cup D\}, k \in K,$$

$$q^{\alpha,s}\text{free}, \quad \forall \alpha \in \bar{A}_s \cup \underline{A}_s, s \in \{T \cup S \cup D\}, \text{and}$$

$$w_b \geq 0, \quad \forall b \in B.$$

Robust-adaptive treatment planning is also performed as described in Algorithm 1 where the robust-adaptive model is solved instead of nominal model in Step 7.

## 3. Experiments and Results

### *3.1. Clinical Example and Computational Setting*

We next use images from one clinical lung cancer case to present the results of the four models (static, nominal-adaptive, robust-adaptive, and robust optimization). The patient in this case underwent four-dimensional CT imaging as a part of a routine treatment simulation before RT. Target volumes and normal structures were manually contoured on the axial slices of the planning CT scan by a physician. The anatomy was discretized into voxels of 2.5 mm $\times$ 2.5 mm $\times$ 2.5 mm. GTV-to-clinical target volume margins of 5 mm were applied, the internal target volume concept was used to account for breathing motion, and margins of 8 mm were added for generation of the PTV from the internal target volume. For simulation of ART, at each adaptation point, PTVs were generated analogously on the basis of the residual tumor volume for each estimated tumor volume. PTV includes the GTV, and an additional margin for possible microscopic disease (MD) extension that may not be visible in the images, and a margin to account for both organ motion and daily setup error. So, we refer to MD the PTV region excluding the GTV. Table 1 shows volumes of interest and the number of voxels within each volume. Figure 3 displays the structures and contours

on the planning CT images. As shown in Figure 3, the tumor is located within the right lung (RL) of this patient.

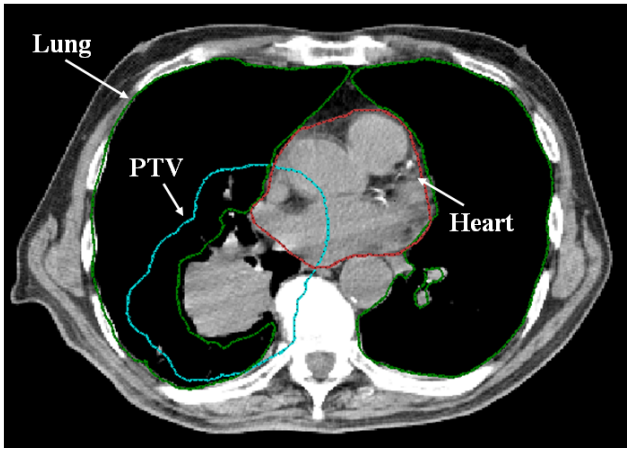


Figure 3: Planning computed tomography image used for the first treatment fraction (PTV, planning target volume)

Table 1: Volumes of interest and the number of voxels within each volume

| Structure | Structure description | Number of voxels |
|---|---|---|
| Planning target volume | Target | 59,030 |
| Heart | Organ at risk | 43,180 |
| Right lung | Organ at risk | 146,698 |
| Total lung | Organ at risk | 287,616 |

Treatments were delivered using seven fixed coplanar photon beams at angles of $0°$, $30°$, $150°$, $180°$, $210°$, $240°$, and $270°$. A prescription dose of 70 Gy for 35 fractions (2 Gy/fraction) was used. Table 2 lists the dose-volume requirements for all volumes of interest. Note that it is possible to miss a subregion of MD by administration of treatment plans adapting to the shrinking tumor. As a result, MD may receive a lower radiation dose with ART than with a nonadaptive treatment plan. Hence, using an ART-based treatment plan can result in an increased risk of local recurrence. To address this concern, one can add a constraint to the optimization model (7) to specify the minimum dose that areas of MD must receive (Gomez and Chang, 2011), where $D$ represents the set of MD voxels in the optimization model.

In our implementation, we minimized the average dose delivered to the healthy tissue in the objective function. We added lower and upper $\alpha$-CVaR constraints on the target to control underdosage and overdosage within the target. In addition, a lower $\alpha$-CVaR constraint was added to MD to ensure that the minimum dose requirement for MD was met. The corresponding coefficients were determined by manual adjustments and are shown in Table 3.

For this paper, we assumed that the treatment plans will be adapted twice over the 7 weeks of treatment, once at the beginning of week 3 and once at the beginning of week 5. These adaptation points were chosen on the basis of a literature review, and they are clinically acceptable for lung cancer treatment. The prescribed dose is divided equally between the fractions (2 Gy/fraction).

To have a more comprehensive evaluation of risk-based models, we also generated a plan using a conventional RO model based on worst-case scenarios (See more details in Appendix C). The generated plan was reviewed in addition to the static, nominal-adaptive, and robust-adaptive plans. Therefore, four plans were studied and compared for our clinical case. The first plan was the original plan from the planning CT scan obtained by solving the static model (non-adaptive). This plan was optimized without considering tumor shrinkage. The second plan was the adapted plan in which the PMF of the tumor shrinkage rate consisted of a single PMF (i.e., nominal PMF). This plan is referred to as the nominal-adaptive plan. The third plan was the adapted plan in which uncertainty in the PMF was also considered, referred to as the robust-adaptive plan. The fourth plan was the solution of the conventional worst-case RO model, referred to as the robust plan.

The cumulative doses to the PTV, MD, heart, and lung were reported to evaluate the quality of the treatment plans. The three-dimensional dose distribution was visualized through a dose-volume histogram (DVH). A DVH illustrates the fraction of the volume of a given target or critical structure receiving at least a certain level of the dose. The accumulated doses of all plans were projected onto the structures. We then conducted a series of experiments to measure the quality of the treatment plans. In each experiment, a different tumor shrinkage rate was used to estimate the changes in the tumor volume. Note that the tumor statistics presented throughout the computational experiments are for the residual tumor. All experiments were performed on a Linux-equipped computer with a Xeon Quad 2.8 GHz processor and 16 GB RAM. The linear programming model was solved using CPLEX 12.6.3.

Table 2: Dose-volume requirements for the volumes of interest

| Volume | Constraints |
|---|---|
| Planning target volume | Prescription: 70 Gy |
| Planning target volume | Volume receiving at least the prescription dose: $\geq 95\%$ |
| Microscopic disease | Minimum dose: 50 Gy |
| Heart | Volume receiving doses higher than 45 Gy: $\leq$65% |
| Total lung | Volume receiving doses higher than 20 Gy: $\leq$45% |

Table 3: Values of the coefficients corresponding to the conditional value-at-risk (CVaR) constraints that were used in the optimization

| | Lower CVaR constraint | | Upper CVaR constraint | |
|---|---|---|---|---|
| Structure | $\alpha$ | $L^s_\alpha$(Gy) | $\alpha$ | $U^s_\alpha$(Gy) |
| Planning target volume | 0.98 | 68 | 0.95 | 72.5 |
| Microscopic disease | 0.99 | 55 | - | - |

### *3.2. Generating Tumor Shrinkage Data*

In our implementation, six representative rates based on historical data from the literature were used to model the nominal PMF of the shrinkage rate, as discussed in Section 2.3.1. However, the uncertainty set in the robust formulation allowed the realized PMF to differ from the nominal PMF

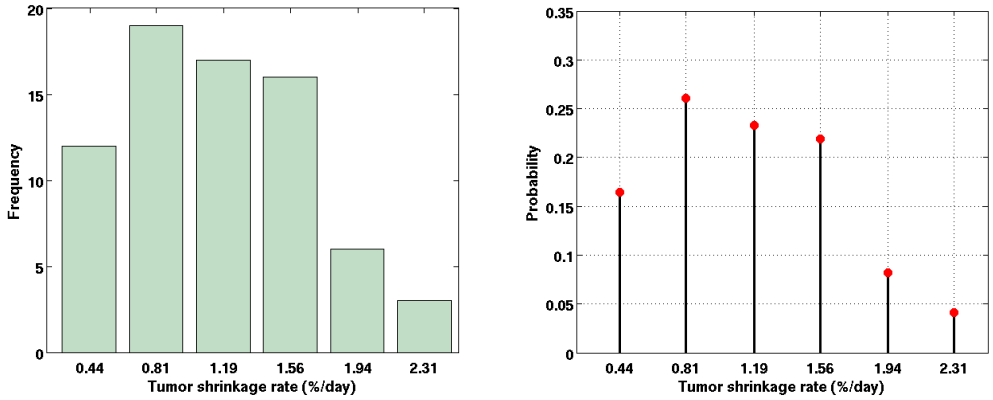


(a) (b)

Figure 4: Tumor shrinkage rate distribution: (a) frequency of occurrence in each interval and (b) nominal probability mass function

for each shrinkage estimate. Figure 4 shows the frequency of occurrence of each shrinkage rate interval (Figure 4a) and the nominal PMF of the shrinkage rate (Figure 4b).

To generate tumor shrinkage data, we assumed that the tumor location was stable over time but that the tumor size could vary. This assumption is in agreement with the findings of Aerts et al. (2008). At each adaptation point (at the beginning of weeks 3 and 5), the number of voxels to be removed for each estimate was calculated on the basis of the tumor shrinkage rate and the number of elapsed days. For example, if the plan was adapted 14 days after treatment began (the first adaptation point), residual tumor volumes corresponding to shrinkage rates of 0.44%, 0.81%, 1.19%, 1.56%, 1.94%, and 2.31% were generated by reducing the tumor volume to 93.84%, 88.66%, 83.34%, 78.16%, 72.84%, and 67.66% of its original volume, respectively. Figure 5 shows the PTVs of six tumor volume estimates used at the first adaptation point with six different colors. For the RO model in (7), the uncertainty set for the tumor shrinkage rate probability was chosen to be the set of all PMFs that had a probability within $\pm 0.10$ of the nominal PMF for each shrinkage rate, which covers the majority of shrinkage cases. The dose deposition matrices for all estimates were generated using the Computational Environment for Radiotherapy Research (CERR) system.

### *3.3. Results*

#### *3.3.1. Dosimetric comparison*

We examined the performance of all four plans in terms of healthy tissue sparing using three OARs: heart, RL, and total lung excluding the GTV (TL). DVHs for these OARs obtained from each plan are depicted in Figure 6. Both of the adaptive plans and the robust plan reduced the volume of lung receiving a high (50 Gy) dose of radiation by approximately 10% compared to the static plan. Similarly, the reductions at 60 and 70 Gy were close to 15% and 10%, respectively. We observed that the difference among nominal-adaptive, robust-adaptive, and robust plans was rather negligible for the lungs. However, both adaptive plans performed better for the heart than did the static plan or the robust plan at 60 and 70 Gy.

To more comprehensively compare the plans with respect to OAR sparing, we collected several

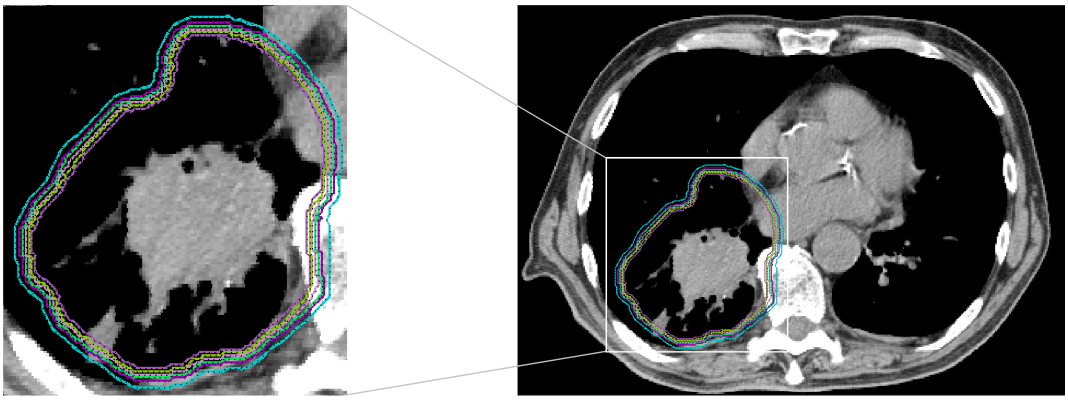

Figure 5: Six different estimates of the planning target volume at the first adaptation point

dose statistics from the DVHs of the OARs, as summarized in Table 4. For comparison purposes, the mean lung dose and the percentage of the total lung volume receiving a dose greater than 20 Gy ($V_{20}$) were used for parallel organs such as RL and TL, while $V_{45}$ and $V_{50}$ statistics were used for a serial organ such as the heart. The average tumor dose statistics from all experiments are summarized in Table 4: the dose delivered to 99% of the PTV ($D_{99}$), the treatment dose delivered to 1% of the PTV ($D_1$), and the volume of PTV receiving the prescribed dose ($V_{70}$).

*Heart:* Both of the adaptive CVaR plans performed similarly with regard to heart sparing in terms of $V_{45}$ and $V_{50}$. Both adaptive plans outperformed the CVaR static plan and the robust plan. For example, the nominal-adaptive and robust-adaptive plans showed 18.28% and 24.5% improvements over the static plan in sparing the heart at $V_{45}$ and $V_{50}$, respectively. In addition, the adaptive plans resulted in 12.72% and 24.5% improvements over the robust plan for the same measures.

*Right Lung:* The nominal-adaptive plan reduced the mean dose to the RL by 14.62% in comparison to the static plan. Similarly, the robust-adaptive plan reduced the dose to the RL by 12.25%, and the robust plan reduced it by 17.18%. In terms of $V_{20}$, the robust plan performed better than the adaptive plans for the RL, reducing the dose by 3.21% (compared to the robust-adaptive plan) and 3.14% (compared to the nominal-adaptive plan).

*Total Lung:* The nominal-adaptive and robust-adaptive plans outperformed the static and robust plans in terms of mean TL dose. In comparison to the static plan, the nominal-adaptive plan reduced the mean dose to TL by 14.99%, while the robust-adaptive plan reduced it by 12.75%. In comparison to the robust plan, the nominal-adaptive plan reduced the mean dose to TL by 6.23%, while the robust-adaptive plan reduced it by 3.76%. It is important to note that the mean lung dose is the basis for estimating pulmonary toxicity (Guckenberger et al., 2011a). Hence, the risk-based plans, such as the robust-adaptive and nominal-adaptive plans, showed the potential to reduce pulmonary toxicity more effectively than the static plan and robust plan.

As seen in Table 4, both of the adaptive plans outperformed the other two methods (static plan and robust plan) for the heart and the lungs. Indeed, the two adaptive plans attained the same $V_{50}$ and $V_{45}$ for the heart. Therefore, we claim that the nominal-adaptive and robust-adaptive plans had approximately the same OAR-sparing ability for the test case discussed in this paper and that they outperformed the (worst-case) robust plan and the static plan.

*Microscopic Disease:* For areas of MD, the volume of MD receiving the minimum dose re-

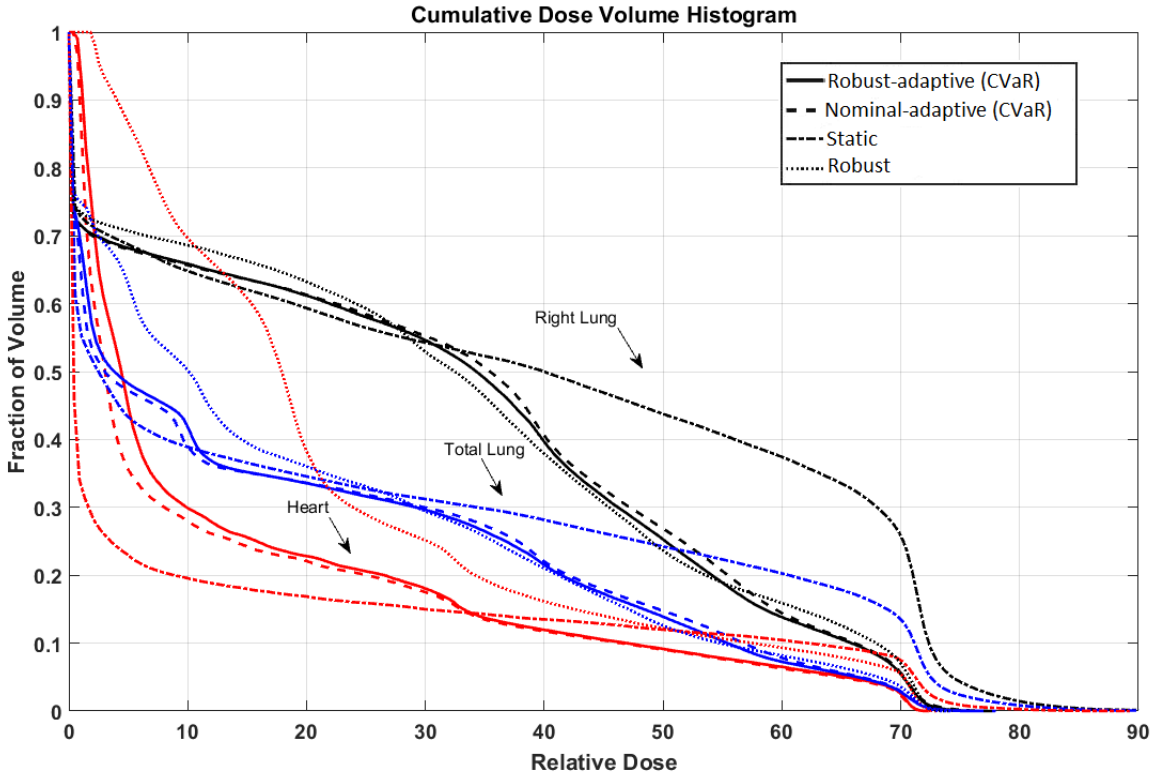


Figure 6: Organ-at-risk dose-volume histograms obtained from the static, nominal-adaptive, robust-adaptive, and robust plans

quirement ($V_{50}$) along with the volume receiving 60 Gy ($V_{60}$) were used to compare the performance of the four plans. Table 4 shows that all four plans delivered the prescribed dose of at least 50 Gy to areas of MD (i.e., $V_{50} = 100\%$ for all plans). Furthermore, the proportion of the MD areas receiving more than 60 Gy ($V_{60}$) was above 99.37% in all plans. These results can be explained by the fact that ART does not compromise dose coverage (and tumor control probability) of volumes of potential MD.

*Planning Target Volume:* Next, we examined the advantage of the robust-adaptive plan in terms of PTV coverage and variability reduction (Table 4). The average PTV receiving the prescribed dose ($V_{70}$) was at 98.98% in the static plan, 94.86% in the nominal-adaptive plan, 96.16% in the robust-adaptive plan, and 94.36% in the robust plan. Therefore, the CVaR plans performed better in terms of PTV coverage than did the robust plan.

As shown in Table 4, the average difference between $D_1$ and $D_{99}$ was 3.12 Gy in the nominal-adaptive plan, 2.82 Gy in the robust-adaptive plan, and 3.86 Gy in the robust plan. More detail about these differences can be found in Figure 7, which depicts the differences between $D_1$ and $D_{99}$ for 35 shrinkage scenarios. These results indicate that the robust-adaptive plan achieved more uniform dose distribution on the PTV than did the nominal-adaptive and robust plans.

Next, we conducted a series of experiments to compare the quality of the treatment plans generated by the four treatment planning methods. Different tumor shrinkage rates were used to estimate residual tumor volume in 35 scenarios. Figure 8 shows 35 target DVHs associated with the 35 scenarios, resulting in DVH clouds (Chu et al., 2005) for each plan. This figure includes

Table 4: Dose-volume parameter comparisons of the static, nominal-adaptive, robust-adaptive, and robust plans ($D_x$ denotes $x\%$ of the structure received at least $D_x$ Gy; $V_x$ denotes the fraction of volume that received at least $x$ Gy)

| | CVaR models | | | |
|---|---|---|---|---|
| Structure | Static | Nominal-adaptive | Robust-adaptive | Robust |
| PTV | | | | |
| $V_{70}(\%)$ | $98.98 \pm 0.1$ | $94.86 \pm 0.70$ | $96.16 \pm 0.46$ | $94.36 \pm 0.65$ |
| $D_1$ (Gy) | $72.61 \pm 0.11$ | $72.53 \pm 0.01$ | $72.42 \pm 0.01$ | $73.24 \pm 0.03$ |
| $D_{99}$ (Gy) | $70.07 \pm 0.04$ | $69.41 \pm 0.21$ | $69.60 \pm 0.1$ | $69.38 \pm 0.07$ |
| MD | | | | |
| $V_{50}(\%)$ | $100 \pm 0.0$ | $100 \pm 0.0$ | $100 \pm 0.0$ | $100 \pm 0.0$ |
| $V_{60}(\%)$ | $99.63 \pm 0.001$ | $99.37 \pm 0.002$ | $99.53 \pm 0.001$ | $99.97 \pm 0.008$ |
| Heart | | | | |
| $V_{45}(\%)$ | 12.85 | 10.50 | 10.50 | 13.50 |
| $V_{50}(\%)$ | 12.00 | 9.06 | 9.07 | 12.00 |
| Right Lung | | | | |
| Mean(Gy) | 36.65 | 31.29 | 32.16 | 30.35 |
| $V_{20}(\%)$ | 59.35 | 61.23 | 61.19 | 63.22 |
| Total Lung | | | | |
| Mean(Gy) | 21.41 | 18.20 | 18.68 | 19.41 |
| $V_{20}(\%)$ | 34.56 | 33.60 | 33.55 | 35.81 |

a $\pm$ b denotes mean $\pm$ standard deviation of the metrics over all experiments.

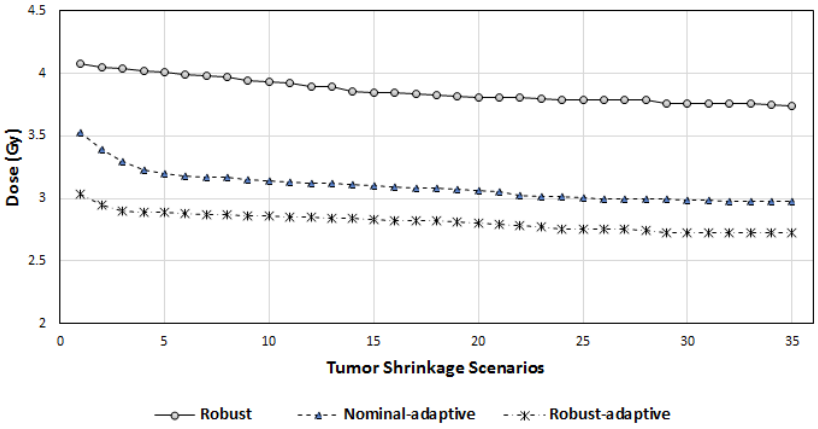


Figure 7: Plot of $(D_1 - D_{99})$ from nominal-adaptive, robust-adaptive, and robust plans for 35 tumor shrinkage scenarios

target coverage corresponding to the CVaR static plan (Figure 8a), the CVaR nominal-adaptive plan (Figure 8b), the CVaR robust-adaptive plan (Figure 8c), and the robust plan (Figure 8d) for all experiments. The vertical line at 70 Gy indicates the prescribed dose for the target. In the target DVH clouds of the four plans, the robust-adaptive plan shows the sharpest dose falloff, followed by the nominal-adaptive plan. This implies that the robust-adaptive plan does very well in the presence of uncertain shrinkage rates.

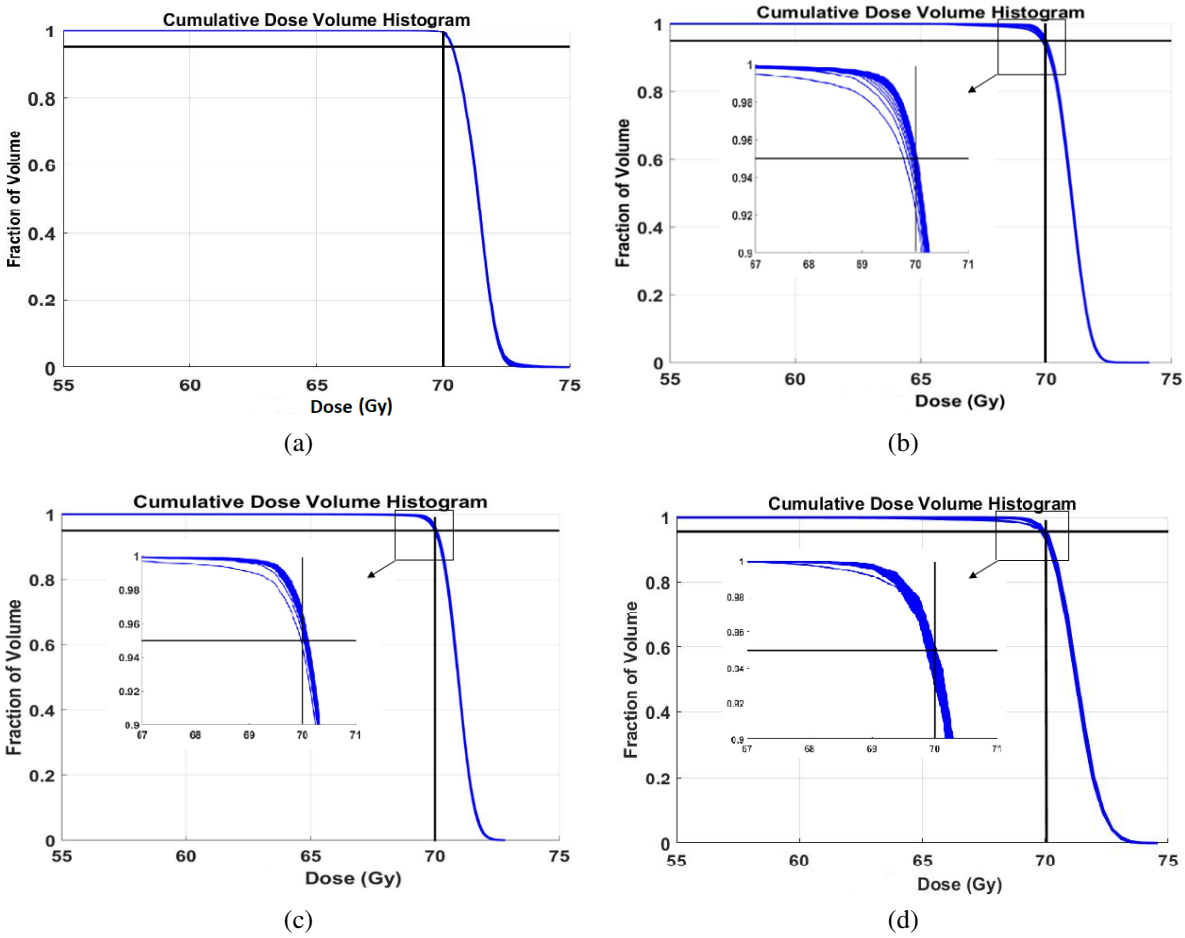


Figure 8: Planning target volume dose-volume histograms for the (a) static, (b) nominal-adaptive, (c) robust-adaptive, (d) robust plans

### *3.3.2. Variability Reduction in DVH*

A clinically acceptable RT plan for a lung cancer case should have more than 95% of the PTV receiving a dose of 70 Gy or more (i.e., the prescription dose). In Figure 8, three of the panels show multiple DVHs according to the various scenarios considered in the experiment. Most plans performed well on PTV coverage, with the robust-adaptive plan having an edge on reducing the fraction of PTV receiving a high dose of radiation (i.e., hot spots). We further expanded DVH lines around the target prescription point or reference point $(70_{Gy}, 0.95)$, as shown in Figure 8 (b), (c), and (d). Ideally, a DVH of the PTV should pass through the reference point, meaning that 95% of the PTV should receive a dose of 70 Gy. A wider dose cloud near this point means a larger deviation from the prescription dose, which may result in an underdose and/or an overdose when delivered as planned. We observed several points regarding the comparison of the DVHs in Figure 8. First, the robust-adaptive plan (c) exhibited a narrower DVH cloud around the target prescription point than did the other plans. Hence, the CVaR-based robust-adaptive plan performed well in reducing variability in the worst-case scenarios. Second, more DVH lines of the nominal-adaptive plan fell below point $(70_{Gy}, 0.95)$ than did those of its robust-adaptive counterpart. This supports the conclusion that using a CVaR model helps reduce worst-case outcome variability.

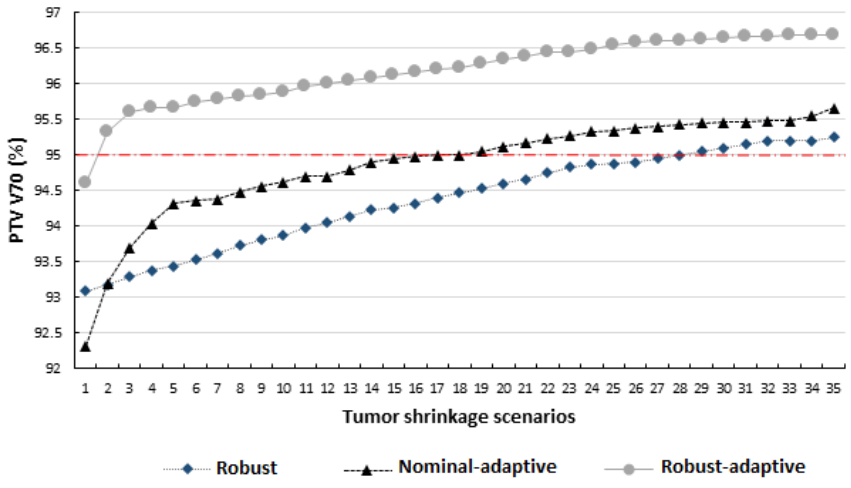


Figure 9: Planning target volume (PTV) coverage ($V_{70}$) for each tested tumor shrinkage scenario

The number of violated scenarios (i.e., scenarios that fell below the reference point) was 15 (43%) for the nominal-adaptive plan and 25 (71%) for the robust plan. Figure (9) also shows $V_{70}$ for PTV in each scenario. Even though the nominal-adaptive plan was based on CVaR, it had many more violations than did the robust-adaptive plan. In robust CVaR, setting the model parameter value of $\alpha$ to 95% (0.95) ensures that at most 5% of the scenarios can be violated in the worst cases. As expected, only one (3%) of the 35 scenarios was violated for the robust-adaptive plan. This plan, therefore, delivered the fewest violations among all methods evaluated in this paper.

*3.3.3. Variability Reduction Comparisons Using Variability Measures*

In general, standard deviation (SD) and median are two commonly used variability measures in statistics. We further included median absolute deviation (MAD) and interquartile range (IQR) to examine the spread of the outcomes in this section (See more details in Appendix D and E). In Figure 10, box plots show the variability in the PTV receiving the prescribed dose ($V_{70}$) for the robust, nominal-adaptive, and robust-adaptive plans.

Both adaptive plans exhibited a narrower IQR than did the robust plan. This can be interpreted as evidence that the adaptive plans perform better than the robust plan in reducing variability in meeting the dose prescription. Furthermore, the upper quartile of the robust-adaptive plan is smaller than that of the nominal-adaptive plan. This suggests that the robust-adaptive plan is more likely to ensure $V_{70}$, that is, to satisfy the prescription dose, than is the nominal-adaptive plan. The robust-adaptive plan also had a narrower IQR than the other plans.

An overall summary of variability measures for the three plans is shown in Table 5. In the first two rows, which show the median and mean values of the plans, a higher value (above 95) is better. In the next three rows, which show measures of variability, a smaller value is better. The robust-adaptive plan outperformed the other plans in all five measures. It is clear that using a CVaR-based model reduced the variability in the plans' meeting the reference point of $(70_{Gy}, 0.95)$. Therefore, we claim that using a risk-based model not only ensures PTV coverage improvement, but also achieves a plan with a lower risk of undesired outcomes.

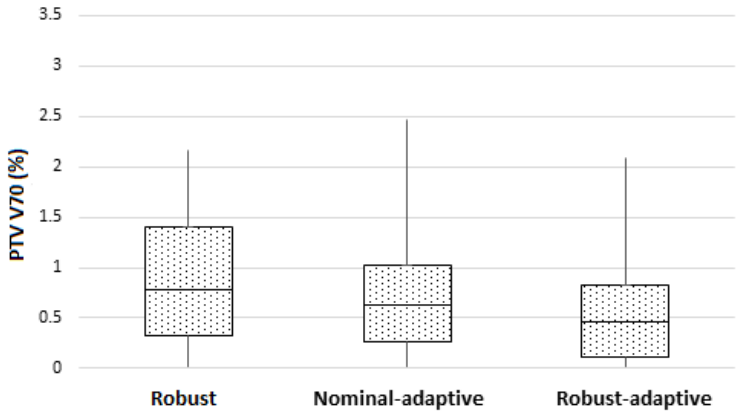


Figure 10: Box plots showing the percentage of the planning target volume (PTV) receiving the prescribed dose of 70 Gy ($V_{70}$) for the robust, nominal-adaptive, and robust-adaptive plans

Table 5: Comparison of variability statistics for nominal-adaptive, robust-adaptive, and robust plans

| | CVaR models | | |
|---|---|---|---|
| | Nominal-adaptive | Robust-adaptive | Robust plan |
| Median | 95.025 | 96.220 | 94.470 |
| Mean | 94.865 | 96.160 | 94.369 |
| IQR | 0.755 | 0.720 | 1.085 |
| MAD | 0.405 | 0.380 | 0.530 |
| SD | 0.701 | 0.461 | 0.658 |

## 4. Conclusion

In this paper, we proposed a risk-based method that combines adaptive and robust optimization in RT treatment planning for lung cancer under tumor shrinkage uncertainty. In this method, CVaR constraints were used as a risk management tool to minimize the large variability in the worst-case scenarios. The benefits of our risk-based robust-adaptive planning approach over robust optimization and static methods were tested in one clinical lung cancer case. A linear programming formulation was solved at each adaptation point to reoptimize the treatment plan and to design an adaptive plan. This adaptive plan considers the response of the tumor to treatment up to a particular point in time during a treatment course. Our results for a clinical lung cancer case showed that this approach achieved less dose variability under various worst-case scenarios, while delivering the prescribed dose to the tumor target and sparing organs at risk. Therefore, we were able to reduce dose variability without compromising the target dose coverage. Our results also showed that the proposed approach can improve dose homogeneity and target coverage. Overall, our experiments suggested that the robust-adaptive model produces adaptive plans that can spare healthy tissue while maintaining the prescribed dose to the target. The robust-adaptive plan showed clinically acceptable delivered dose to OARs while achieving better PTV coverage and a more homogeneous dose distribution on the PTV.

An an extension of this work, one could collect and analyze a large image data set from patients who have completed treatments, and use machine learning techniques to develop a dynamic tumor

shrinkage model to improve the accuracy of predicting tumor volume reduction.

## Appendix A. Static Model Formulation (Chan et al., 2014)

Let $L_s^\alpha$ denote a lower bound on target structures for $\alpha \in \underline{A}_s$, where $\underline{A}_s$ is a set of lower $\alpha$ levels, and let $U_s^\alpha$ denote upper bounds on structure $s$ for $\alpha \in \bar{A}_s$, where $\bar{A}_s$ is a set of all upper $\alpha$ levels. The static model using CVaR is

$$\min \quad \sum_{s\in T\cup S} \frac{C_s}{|V_s|} \sum_{v\in V_s} \sum_{b\in B} \Delta_{v,b} w_b \tag{A.1a}$$

s.t.

$$\bar{\zeta}_s^\alpha + \frac{1}{(1-\alpha)|V_s|} \sum_{v\in V_s} \bar{d}_{v,\alpha}^s \le U_s^\alpha, \quad \forall \alpha \in \bar{A}_s, s \in T\cup S, \tag{A.1b}$$

$$\bar{d}_{v,\alpha}^s \ge \sum_{b\in B} \Delta_{v,b} w_b - \bar{\zeta}_s^\alpha, \quad \forall v \in V_s, \alpha \in \bar{A}_s, s \in T\cup S,$$

$$\underline{\zeta}_s^\alpha - \frac{1}{(1-\alpha)|V_s|} \sum_{v\in V_s} \underline{d}_{v,\alpha}^s \ge L_s^\alpha, \quad \forall \alpha \in \underline{A}_s, s \in T\cup D, \tag{A.1c}$$

$$\underline{d}_{v,\alpha}^s \ge \underline{\zeta}_s^\alpha - \sum_{b\in B} \Delta_{v,b} w_b, \quad \forall v \in V_s, \alpha \in \underline{A}_s, s \in T\cup D,$$

$$\bar{\zeta}_s^\alpha \ge 0, \quad \forall \alpha \in \bar{A}_s, s \in T\cup S,$$

$$\bar{d}_{v,\alpha}^s \ge 0, \quad \forall v \in V_s, \alpha \in \bar{A}_s, s \in T\cup S,$$

$$\underline{\zeta}_s^\alpha \ge 0, \quad \forall \alpha \in \underline{A}_s, s \in T\cup D,$$

$$\underline{d}_{v,\alpha}^s \ge 0, \quad \forall v \in V_s, \alpha \in \underline{A}_s, s \in T\cup D, \text{and}$$

$$w_b \ge 0, \quad \forall b \in B.$$

Note that the CVaR constraints are reformulated as linear constraints by replacing the terms $[t]^+$ with auxiliary variables. The objective function in (A.1a) minimizes the summation of the average dose to all structures. Constraint (A.1b) ensures that the average dose received by the subset of structure $s$ of relative volume $1-\alpha$ receiving the highest amount of the dose is no more than $U_\alpha^s$. Constraint (A.1c) guarantees that the average dose received by the subset of a target of relative volume $1-\alpha$ receiving the lowest amount of dose is at least equal to $L_\alpha^s$.

## Appendix B. Nominal Model Formulation (Chan et al., 2014)

The nominal model using the nominal PMF of the instances is

$$\min \quad \sum_{k\in K} \sum_{s\in T\cup S} \frac{C_s}{|V_s^k|} \sum_{v\in V_s^k} \sum_{b\in B} \Delta_{v,k,b} p(k) w_b \tag{B.1}$$

s.t.

$$\bar{\zeta}_s^\alpha + \frac{1}{1-\alpha} \sum_{k\in K} \sum_{v\in V_s^k} \bar{d}_{v,k,\alpha}^s \frac{p(k)}{|V_s^k|} \le U_s^\alpha, \quad \forall \alpha \in \bar{A}_s, s \in T\cup S,$$

$$\bar{d}_{v,k,\alpha}^s \ge \sum_{b\in B} \Delta_{v,k,b} w_b - \bar{\zeta}_s^\alpha, \quad \forall v \in V_s^k, \alpha \in \bar{A}_s, s \in T\cup S, k \in K,$$

$$\underline{\zeta}_s^{\alpha} - \frac{1}{1-\alpha} \sum_{k \in K} \sum_{v \in V_s^k} \underline{d}_{v,k,\alpha}^{s} \frac{p(k)}{|V_s^k|} \geq L_s^{\alpha}, \quad \forall \alpha \in \underline{A}_s, s \in T \cup D,$$

$$\underline{d}_{v,k,\alpha}^{s} \geq \underline{\zeta}_s^{\alpha} - \sum_{b \in B} \Delta_{v,k,b} w_b, \quad \forall v \in V_s^k, \alpha \in \underline{A}_s, s \in T \cup D, k \in K,$$

$$\bar{\zeta}_s^{\alpha} \geq 0, \quad \forall \alpha \in \bar{A}_s, s \in T \cup S,$$

$$\bar{d}_{v,k,\alpha}^{s} \geq 0, \quad \forall v \in V_s^k, \alpha \in \bar{A}_s, s \in T \cup S, k \in K,$$

$$\underline{\zeta}_s^{\alpha} \geq 0, \quad \forall \alpha \in \underline{A}_s, s \in T \cup D,$$

$$\underline{d}_{v,k,\alpha}^{s} \geq 0, \quad \forall v \in V_s^k, \alpha \in \underline{A}_s, s \in T \cup D, k \in K, \text{and}$$

$$w_b \geq 0, \quad \forall b \in B.$$

## Appendix C. Robust Optimization Model Formulation (Zaghian et al., 2017a)

The worst-case robust optimization model is

$$\begin{aligned} \min \quad & f(D) = C_T \left\| (D_v^{pt} - D_v^T)_+ \right\|_1 + C_S \left\| (D_v^S - D_v^{ps}) \right\|_1 \\ \text{s.t.} \quad & \\ & L_v \leq D_v^k \leq U_v, \qquad \forall\, v \in V_s,\ s \in T \cup S,\ k \in K, \\ & w_b \geq 0, \qquad \forall\, b \in B, \end{aligned}$$

where $D_v^{pt}$ is the prescription dose for each voxel of the tumor; $D_v^{ps}$ is the prescription dose for the OAR voxels; $L_v$ and $U_v$ are the dose lower and upper bounds for each voxel $v$ in the structure $s$, respectively. In this model, $D_v^k$ is the total dose that a voxel $v$ receives under scenario $k$, $D_v^T$ is the minimum dose of a voxel inside the target, and $D_v^S$ is the maximum dose of a voxel inside the OAR structures. These dose variables can be calculated as follows

$$D_v^k = \sum_{b \in B} \Delta_{v,k,b}\, w_b, \qquad \forall\, v \in V_s,\ s \in T \cup S,\ k \in K,$$

$$\begin{aligned} D_v^T &= min\ \ D_v^k, \qquad \forall\, v \in V_s,\ s \in T,\ k \in K, \\ D_v^S &= max\ \ D_v^k, \qquad \forall\, v \in V_s,\ s \in S,\ k \in K. \end{aligned}$$

## Appendix D. Interquartile Range (IQR)

IQR can be calculated by subtracting the first quartile ($Q_1$) from the third quartile ($Q_3$) as follows:

$$IQR = Q_3 - Q_1.$$

## Appendix E. Median Absolute Deviation (MAD)

MAD is calculated by finding the median of the absolute deviations around the median of $V_{70}$ for all 35 scenarios, as follows:

$$MAD = median(|V_{70}^k - median(\boldsymbol{V_{70}})|),$$

where $V_{70}^k$ is the percentage of the planning target volume (PTV) receiving the prescribed dose of 70 Gy ($V_{70}$) in the $k^{th}$ shrinkage scenario and $\boldsymbol{V_{70}}$ is the vector of $V_{70}$s.

## Appendix F. Nomenclature

Table F.1: Notation

| Notations | Description |
|---|---|
| Sets | |
| $B$ | Set of all beamlets |
| $T$ | Set of target structures |
| $S$ | Set of OAR structures |
| $D$ | Set of MD |
| $V_s$ | Set of voxels of structure $s$ |
| $\underline{A}_s$ | Set of all lower $\alpha$ levels |
| $\bar{A}_s$ | Set of all upper $\alpha$ levels |
| $K$ | Set of tumor shrinkage scenarios |
| $V_s^k$ | Set of voxels in structure $s$ for scenario $k$ |
| Indices | |
| $b$ | Index for beamlets |
| $s$ | Index for structures ($s \in \{T \cup S\}$) |
| $v$ | Index for voxels |
| $k$ | Index for tumor shrinkage scenario |
| Primary decision variables | |
| $w_b$ | Intensity of radiation delivered by beamlet b |
| $D_v$ | Total dose delivered to voxel $v$ |
| Other variables | |
| $\bar{\zeta}_s^\alpha$ | The upper $\alpha$-VaR for structure $s$ |
| $\underline{\zeta}_s^\alpha$ | The lower $\alpha$-VaR for structure $s$ |
| $\bar{\phi}_s^\alpha(\mathbf{w})$ | The upper $\alpha$-CVaR for structure $s$ |
| $\underline{\phi}_s^\alpha(\mathbf{w})$ | The lower $\alpha$-CVaR for structure $s$ |
| $r_k^{\alpha,s}$ | Dual counterpart variable |
| $q^{\alpha,s}$ | Dual counterpart variable |
| $\bar{d}_{v,\alpha}^s$ | Auxiliary variable for upper CVaR constraint |
| $\underline{d}_{v,\alpha}^s$ | Auxiliary variable for lower CVaR constraint |
| $\bar{d}_{v,k,\alpha}^s$ | Auxiliary variable for upper CVaR constraint for scenario $k$ |
| $\underline{d}_{v,k,\alpha}^s$ | Auxiliary variable for lower CVaR constraint for scenario $k$ |
| Parameters | |
| $\Delta_{v,b}$ | The element of the dose deposition matrix |
| $\Delta_{v,k,b}$ | The element of the dose deposition matrix for scenario $k$ |
| $\lvert V_s \rvert$ | Number of voxels in structure $s$ |
| $\lvert V_s^k \rvert$ | The number of voxels in structure $s$ for scenario $k$ |
| $L_s^\alpha$ | The dose lower bound on target structures for $\alpha \in \underline{A}_s$ |
| $U_s^\alpha$ | The dose upper bound on structure $s$ for $\alpha \in \bar{A}_s$ |
| $C_s$ | The cost for structure $s$ in objective function |
| $p_k$ | Probability of tumor shrinkage scenario $k$ |
| $\bar{p}(k)$ | The upper bound for probability of scenario $k$ |
| $\underline{p}(k)$ | The lower bound for probability of scenario $k$ |

## References


Aerts, H. J., Bosmans, G., van Baardwijk, A. A., Dekker, A. L., Oellers, M. C., Lambin, P., and De Ruysscher, D. (2008). Stability of $^{18}$F-deoxyglucose uptake locations within tumor during radiotherapy for NSCLC: a prospective study. *International Journal of Radiation Oncology* Biology* Physics*, 71(5):1402–1407.

An, Y., Schild, S. E., Bues, M., Liu, W., and Liang, J. (2017). Robust treatment planning with conditional value at risk chance constraints in intensity-modulated proton therapy. *Medical physics*, 44(1):28–36.

Aven, T. (2016). Risk assessment and risk management: Review of recent advances on their foundation. *European Journal of Operational Research*, 253(1):1–13.

Belfatto, A., Riboldi, M., Ciardo, D., Cecconi, A., Lazzari, R., Jereczek, B. A., Orecchia, R., Baroni, G., and Cerveri, P. (2016). Adaptive mathematical model of tumor response to radiotherapy based on CBCT data. *IEEE Journal of Biomedical and Health Informatics*, 20(3):802–809.

Ben-Haim, Y. (2012). Doing our best: Optimization and the management of risk. *Risk Analysis*, 32(8):1326–1332.

Berkovic, P., Paelinck, L., Lievens, Y., Gulyban, A., Goddeeris, B., Derie, C., Surmont, V., Neve, W. D., and Vandecasteele, K. (2015). Adaptive radiotherapy for locally advanced non-small cell lung cancer, can we predict when and for whom? *Acta Oncologica*, 54(9):1438–1444.

Bortfeld, T., Chan, T. C., Trofimov, A., and Tsitsiklis, J. N. (2008). Robust management of motion uncertainty in intensity-modulated radiation therapy. *Operations Research*, 56(6):1461–1473.

Bortfeld, T., Jokivarsi, K., Goitein, M., Kung, J., and Jiang, S. B. (2002). Effects of intra-fraction motion on IMRT dose delivery: statistical analysis and simulation. *Physics in Medicine and Biology*, 47(13):2203–2220.

Britton, K. R., Starkschall, G., Tucker, S. L., Pan, T., Nelson, C., Chang, J. Y., Cox, J. D., Mohan, R., and Komaki, R. (2007). Assessment of gross tumor volume regression and motion changes during radiotherapy for nonsmall-cell lung cancer as measured by four-dimensional computed tomography. *International Journal of Radiation Oncology* Biology* Physics*, 68(4):1036–1046.

Chan, T. C., Mahmoudzadeh, H., and Purdie, T. G. (2014). A robust-CVaR optimization approach with application to breast cancer therapy. *European Journal of Operational Research*, 238(3):876–885.

Chan, T. C. and Mišić, V. V. (2013). Adaptive and robust radiation therapy optimization for lung cancer. *European Journal of Operational Research*, 231(3):745–756.

Chan, T. C. Y., Bortfeld, T., and Tsitsiklis, J. N. (2006). A robust approach to IMRT optimization. *Physics in Medicine & Biology*, 51(10):2567–83.

Chen, W., Unkelbach, J., Trofimov, A., Madden, T., Kooy, H., Bortfeld, T., and Craft, D. (2012). Including robustness in multi-criteria optimization for intensity-modulated proton therapy. *Physics in Medicine & Biology*, 57(3):591–600.

Chu, M., Zinchenko, Y., Henderson, S. G., and Sharpe, M. B. (2005). Robust optimization for intensity modulated radiation therapy treatment planning under uncertainty. *Physics in Medicine and Biology*, 50(23):5463–5477.

Dial, C., Weiss, E., Siebers, J. V., and Hugo, G. D. (2016). Benefits of adaptive radiation therapy in lung cancer as a function of replanning frequency. *Medical Physics*, 43(4):1787.

Erridge, S. C., Seppenwoolde, Y., Muller, S. H., van Herk, M., De Jaeger, K., Belderbos, J. S., Boersma, L. J., and Lebesque, J. V. (2003). Portal imaging to assess set-up errors, tumor motion and tumor shrinkage during conformal radiotherapy of non-small cell lung cancer. *Radiotherapy and Oncology*, 66(1):75–85.

Fox, J., Ford, E., Redmond, K., Zhou, J., Wong, J., and Song, D. Y. (2009). Quantification of tumor volume changes during radiotherapy for nonsmall-cell lung cancer. *International Journal of Radiation Oncology* Biology* Physics*, 74(2):341–348.

Gabrel, V., Murat, C., and Thiele, A. (2014). Recent advances in robust optimization: An overview. *European Journal of Operational Research*, 235(3):471–483.

Gomez, D. R. and Chang, J. Y. (2011). Adaptive radiation for lung cancer. *Journal of Oncology*, 2011:1–10.

Guckenberger, M., Richter, A., Wilbert, J., Flentje, M., and Partridge, M. (2011a). Adaptive radiotherapy for locally advanced nonsmall-cell lung cancer does not underdose the microscopic disease and has the potential to increase tumor control. *International Journal of Radiation Oncology* Biology* Physics*, 81(4):e275–e282.

Guckenberger, M., Wilbert, J., Richter, A., Baier, K., and Flentje, M. (2011b). Potential of adaptive radiotherapy to escalate the radiation dose in combined radiochemotherapy for locally advanced nonsmall cell lung cancer. *International Journal of Radiation Oncology* Biology* Physics*, 79(3):901–908.

Hu, Z., Wei, C., Yao, L., Li, L., and Li, C. (2016). A multi-objective optimization model with conditional value-at-risk constraints for water allocation equality. *Journal of Hydrology*, 542:330–342.

Kardar, L., Li, Y., Li, X., Cao, W., Chang, J., Liao, L., Zhu, R., Sahoo, N., Gillin, M., Liao, Z., Komaki, R., Cox, J., Lim, G., and Zhang, Z. (2014). Evaluation and mitigation of the interplay effects for intensity modulated proton therapy for lung cancer in a clinical setting. *Practical Radiation Oncology*, 3(6):e259–e268.

Khabazian, A., Zaghian, M., and Lim, G. (2019). A feasibility study of a risk-based stochastic optimization approach for radiation treatment planning under setup uncertainty. *Computers and Industrial Engineering*, 135:67–78.

Knap, M. M., Hoffmann, L., Nordsmark, M., and Vestergaard, A. (2010). Daily cone-beam computed tomography used to determine tumour shrinkage and localisation in lung cancer patients. *Acta Oncologica*, 49(7):1077–1084.

Kupelian, P. A., Ramsey, C., Meeks, S. L., Willoughby, T. R., Forbes, A., Wagner, T. H., and Langen, K. M. (2005). Serial megavoltage CT imaging during external beam radiotherapy for nonsmall-cell lung cancer: Observations on tumor regression during treatment. *International Journal of Radiation Oncology* Biology* Physics*, 63(4):1024–1028.

Lee, H., Ahn, Y. C., Oh, D., Nam, H., Kim, Y. I., and Park, S. Y. (2014). Tumor volume reduction rate measured during adaptive definitive radiation therapy as a potential prognosticator of locoregional control in patients with oropharyngeal cancer. *Head & Neck*, 36(4):499–504.

Li, L., Shao, H., Wang, R., and Yang, J. (2018). Worst-case range value-at-risk with partial information. *SIAM J. Finan. Math*, 9(1):190–218.

Li, Y., Kardar, L., Li, X., Li, H., Cao, W., Chang, J., Liao, L., Zhu, R., Sahoo, N., Gillin, M., Lim, G., and Zhang, Z. (2014). On the interplay effects with proton scanning beams in stage iii lung cancer. *Medical Physics*, 41(2):021721.

Lim, G. and Cao, W. (2012). A two-phase method for selecting IMRT treatment beam angles: Branch-and-prune and local neighborhood search. *European Journal of Operational Research*, 217(3):609–618.

Lin, S., Lim, G., and Bard, J. (2016). Benders decomposition and an ip-based heuristic for selecting IMRT treatment beam angles. *European Journal of Operational Research*, 251(3):715–726.

Mišić, V. V. and Chan, T. C. (2015). The perils of adapting to dose errors in radiation therapy. *PloS one*, 10(5):e0125335.

Moazeni, S., Powell, W. B., and Hajimiragha, A. H. (2015). Mean-conditional value-at-risk optimal energy storage operation in the presence of transaction costs. *IEEE Transactions on Power Systems*, 30(3):1222–1232.

Najjarbashi, A. and Lim, G. (2019). A variability reduction method for the operating room scheduling problem under uncertainty using CVaR. *Operations Research for Health Care*, 20:25–32.

Noyan, N. (2012). Risk-averse two-stage stochastic programming with an application to disaster management. *Computers & Operations Research*, 39(3):541–559.

Olafsson, A. and Wright, S. J. (2006). Efficient schemes for robust IMRT treatment planning. *Physics in Medicine and Biology*, 51(21):5621–5642.

Ramella, S., Fiore, M., Silipigni, S., Zappa, M. C., Jaus, M., Alberti, A. M., Matteucci, P., Molfese, E., Cornacchione, P., Greco, C., Trodella, L., Ippolito, E., and DAngelillo, R. M. (2017). Local control and toxicity of adaptive radiotherapy using weekly CT imaging: Results from the LARTIA trial in stage III NSCLC. *Journal of Thoracic Oncology*, 12(7):1122–1130.

Romeijn, H. E., Ahuja, R. K., Dempsey, J. F., and Kumar, A. (2006). A new linear programming approach to radiation therapy treatment planning problems. *Operations Research*, 54(2):201–216.

Romeijn, H. E., Ahuja, R. K., Dempsey, J. F., Kumar, A., and Li, J. G. (2003). A novel linear programming approach to fluence map optimization for intensity modulated radiation therapy treatment planning. *Physics in Medicine and Biology*, 48(21):3521–3542.

Saka, B., Rardin, R. L., Langer, M. P., and Dink, D. (2011). Adaptive intensity modulated radiation therapy planning optimization with changing tumor geometry and fraction size limits. *IIE Transactions on Healthcare Systems Engineering*, 1(4):247–263.

Schoot, A. J., de Boer, P., Visser, J., Stalpers, L. J. A., Rasch, C. R. N., and Bel, A. (2017). Dosimetric advantages of a clinical daily adaptive plan selection strategy compared with a non-adaptive strategy in cervical cancer radiation therapy. *Acta oncologica*, 56(5):667–674.

Siegel, R. L., Miller, K. D., and Jemal, A. (2018). Cancer statistics, 2018. *CA: A Cancer Journal for Clinicians*, 68(1):7–30.

Sir, M. Y., Epelman, M. A., and Pollock, S. M. (2012). Stochastic programming for off-line adaptive radiotherapy. *Annals of Operations Research*, 196(1):767–797.

Stroom, J. C. and Heijmen, B. J. M. (2002). Geometrical uncertainties, radiotherapy planning margins, and the ICRU-62 report. *Radiotherapy and Oncology*, 64(1):75–83.

Summers, T., Warrington, J., Morari, M., and Lygeros, J. (2015). Stochastic optimal power flow based on conditional value at risk and distributional robustness. *International Journal of Electrical Power & Energy Systems*, 72:116–125.

Uryasev, S. (2000). Conditional value-at-risk: optimization algorithms and applications. In *Computational Intelligence for Financial Engineering, 2000. (CIFEr) Proceedings of the IEEE/IAFE/INFORMS 2000 Conference*, pages 49–57. IEEE.

Veresezan, O., Troussier, I., Lacout, A., Kreps, S., Maillard, S., Toulemonde, A., Marcy, P.-Y., Huguet, F., and Thariat, J. (2017). Adaptive radiation therapy in head and neck cancer for clinical practice: state of the art and practical challenges. *Japanese Journal of Radiology*, 35(2):43–52.

Woodford, C., Yartsev, S., Dar, A. R., Bauman, G., and Van Dyk, J. (2007). Adaptive radiotherapy planning on decreasing gross tumor volumes as seen on megavoltage computed tomography images. *International Journal of Radiation Oncology* Biology* Physics*, 69(4):1316–1322.

Zaghian, M., Cao, W., Liu, W., Kardar, L., Randeniya, S., Mohan, R., and Lim, G. (2017a). Comparison of linear and nonlinear programming approaches for worst case dose and minmax robust optimization of intensitymodulated proton therapy dose distributions. *Journal of Applied Clinical Medical Physics*, 18(2):15–25.

Zaghian, M., Lim, G. J., and Khabazian, A. (2017b). A chance-constrained programming framework to handle uncertainties in radiation therapy treatment planning. *European Journal of Operational Research*, 266(2):736–745.

Zarepisheh, M., Long, T., Li, N., Tian, Z., Romeijn, H. E., Jia, X., and Jiang, S. B. (2014). A DVH-guided IMRT optimization algorithm for automatic treatment planning and adaptive radiotherapy replanning. *Medical Physics*, 41(6Part1):061711.

Zheng, Y., Singh, H., Zhao, L., Ramirez, E. V., Rana, S., Prabhu, K., Doh, L. S., and Larson, G. L. (2015). Adaptive radiation therapy for lung cancer using uniform scanning proton beams: Adaptation strategies, practical considerations, and clinical outcomes. *International Journal of Radiation Oncology Biology Physics*, 93(3):S29.